

Electronic Supplementary Information

The bifunctional volcano plot: thermodynamic limits for single-atom catalysts for oxygen reduction and evolution

Manuel Kolb^{*,1}, Federico Calle-Vallejo^{*,1}

¹ Department of Materials Science and Chemical Physics & Institute of Theoretical and Computational Chemistry (IQTCUB), University of Barcelona, Martí i Franquès 1, 08028 Barcelona, Spain.

*Correspondence to: mjkolb@ub.edu, f.calle.vallejo@ub.edu

Contents

S1. Obtaining the scaling relations in Figure 1 of the main text	2
S2. Obtaining the location of the maxima of the volcano plots	3
S3. Functional shape of the Bifunctional Index.....	5
S4. Corrections for the data points in Figure 2 in the main text	6
S5. Discussion of the anomalous datapoints in Figure 2 in the main text	9
S6. Explicit values for ΔG_{OH} , ΔG_{GO} , ΔG_{OOH} , η_{OER} , η_{ORR} and BI, as shown in Figure 2 in the main text	10
S7. References.....	11

S1. Obtaining the scaling relations in Figure 1 of the main text

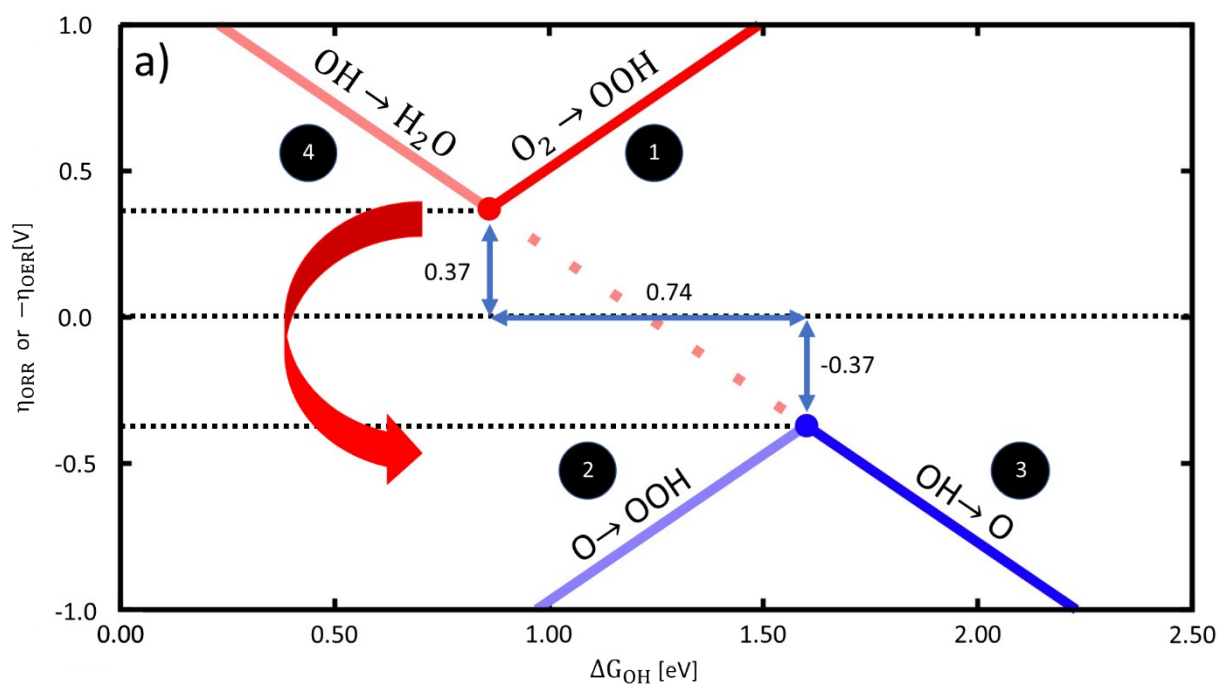
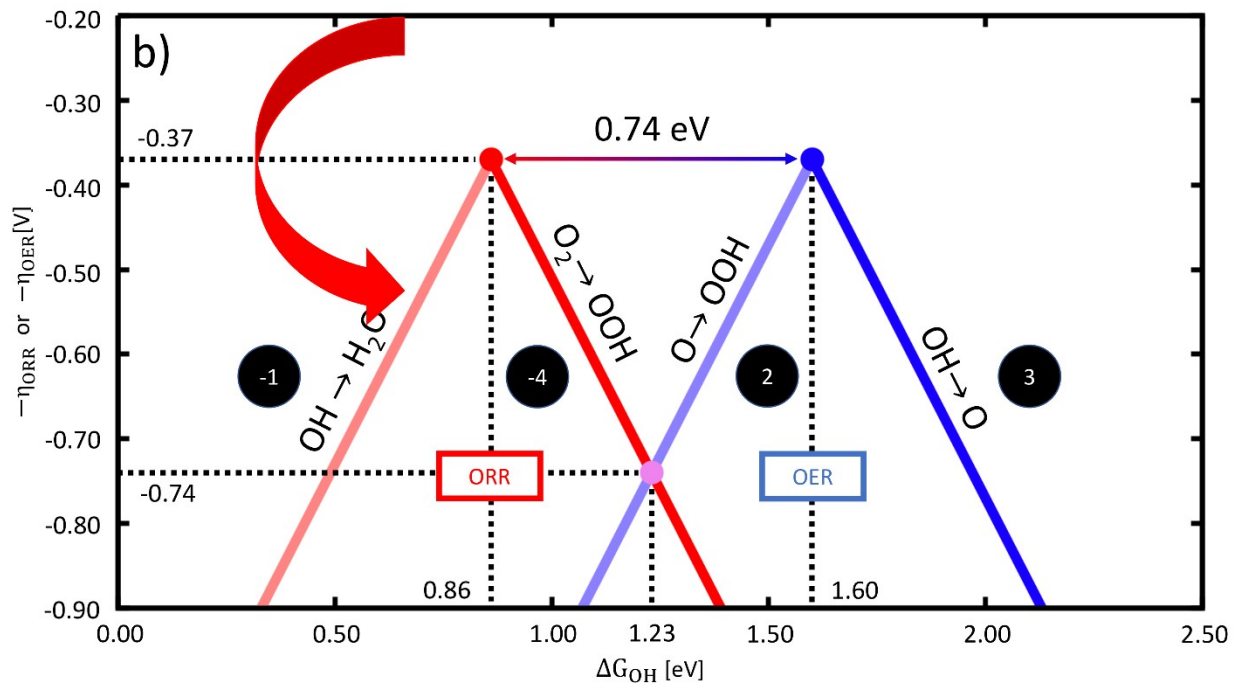


Figure S1. a) Volcano plots based on scaling relations for the ORR and OER, as obtained from scaling relations. The red arrow marks the inversion of the ORR volcano plot, as described in the main text. b) Reproduced Figure 1 from the main text with a red arrow marking the inversion for easier visualization.



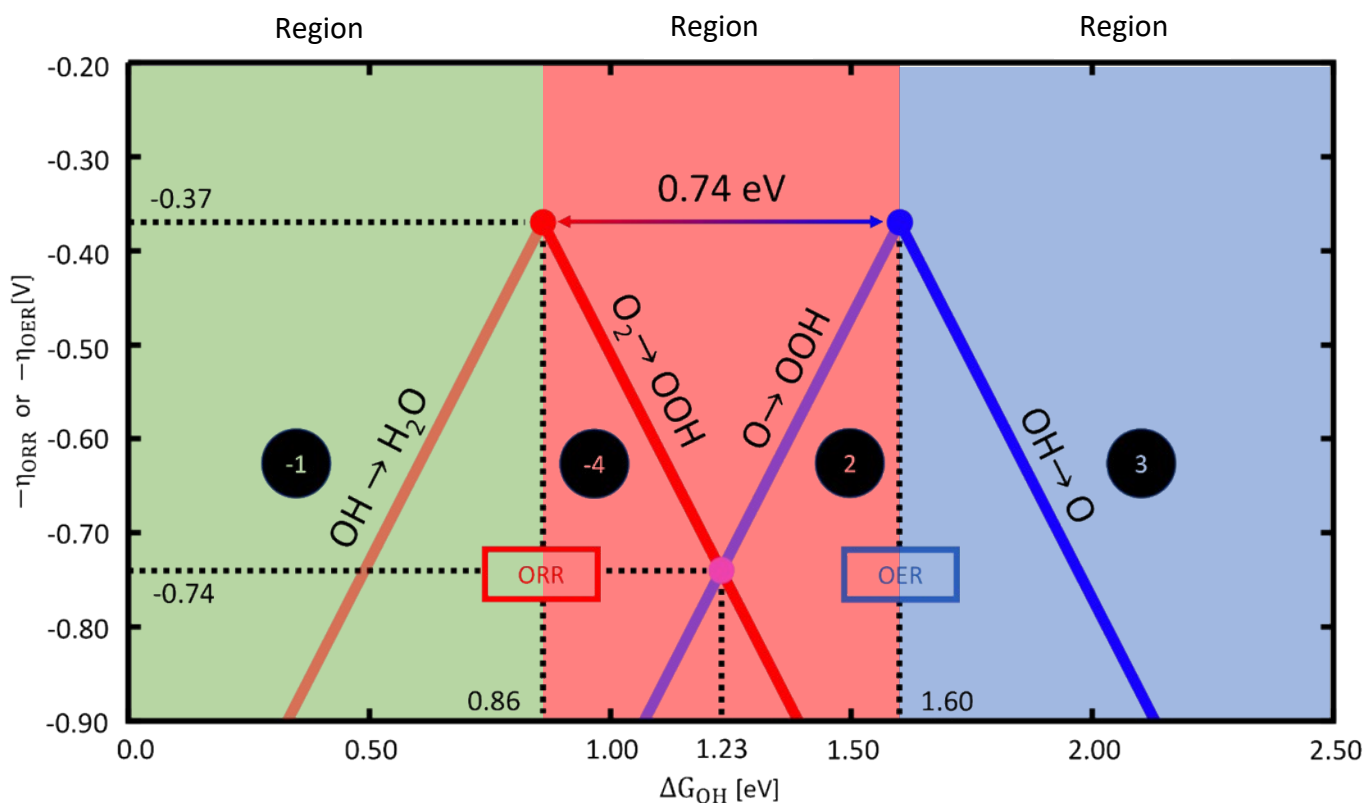


Figure S2. Reproduction of Figure 1 in the main text with regions I, II and III marked as discussed in the text.

S2. Obtaining the location of the maxima of the volcano plots

From previous publications^{1,2} we obtain the mathematical formulation for the scaling relations of the intermediates for the OER/ORR reaction couple (with all energies in eV):

$$\Delta G_{H_2O} = 0 \quad (S1)$$

$$\Delta G_{OH} = \Delta G_{OH} \quad (S2)$$

$$\Delta G_O = \Delta G_O \quad (S3)$$

$$\Delta G_{OOH} = \Delta G_{OH} + 3.20 \quad (S4)$$

$$\Delta G_{O_2} = 4.92 \quad (S5)$$

We note that there is no fixed functional form that can be obtained from first principles for ΔG_O as a function of ΔG_{OH} . From Equations S1-S5, we can now begin to derive the intersections of the two pairs of scaling lines. For the intersection of the lines for the

reaction steps (-1) and (-4) (see the main text), which describes the apex of the overpotential trend for the ORR, we equate the two lines:

$$1.23 V - (\Delta G_{H_2O} - \Delta G_{OH}) = 1.23 V - (\Delta G_{OOH} - \Delta G_{OH}) \quad (S6)$$

and apply the relationships from above to arrive at:

$$1.23 V - (0 - \Delta G_{OH}) = 1.23 V - (\Delta G_{OH} + 3.20 V - \Delta G_{OH}), \quad (S7)$$

which we can then solve to obtain:

$$\Delta G_{OH,intersection,ORR} = 0.86 V \quad (S8)$$

We can follow the same approach to calculate the second intersection for the overpotential of the OER (reaction steps 2 and 3 in the main text):

$$(\Delta G_{OOH} - \Delta G_O) - 1.23 V = (\Delta G_O - \Delta G_{OH}) - 1.23 V \quad (S9)$$

which we can simplify to:

$$(\Delta G_{OH} + 3.20 V - \Delta G_O) - 1.23 V = (\Delta G_O - \Delta G_{OH}) - 1.23 V \quad (S10)$$

which can then be solved for $\Delta G_{OH,intersection,OER}$:

$$\Delta G_{OH,intersection,OER} = \frac{3.20 V}{2} = 1.60 V \quad (S11)$$

We note that to arrive at this value, no explicit form for ΔG_O was needed. Based on the knowledge of the intersections, we can now obtain the functional form of the lines that make up Figure S2, as a function of ΔG_{OH} , assuming that ΔG_O vs ΔG_{OH} has a slope of 2, as predicted from the original discussion on scaling relations by Abild-Pedersen et al:³

$$-\eta_{ORR,-1}(\Delta G_{OH}) = \frac{\Delta G_{OH}}{e} - 1.23 V \quad (S12)$$

$$-\eta_{OER,2}(\Delta G_{OH}) = \frac{\Delta G_{OH}}{e} - 1.97 V \quad (S13)$$

$$-\eta_{OER,3}(\Delta G_{OH}) = -\frac{\Delta G_{OH}}{e} + 1.23 V \quad (S14)$$

$$-\eta_{ORR,-4}(\Delta G_{OH}) = -\frac{\Delta G_{OH}}{e} + 0.49 V \quad (S15)$$

Please note that the minus signs in front of the values for $\eta_{ORR,-1}$ and $\eta_{ORR,-4}$ stem from the inversion of the volcano shown in Figure S1. Equations S12-S15 are plotted to arrive at Figure S2 and Figure 2 in the main text.

In the following, we will derive the intersections of the scaling relations shown in Figure S2. Using the functional forms in Equations S12-S15, we can deduce the values of the overpotential at three important points. First, for the ORR apex at $\Delta G_{OH} = 0.86 \text{ eV}$:

$$-\eta_{OER,-1}(\Delta G_{OH} = 0.86 \text{ eV}) = \left(\frac{0.86 \text{ eV}}{e} - 1.23 \text{ V} \right) = -0.37 \text{ V} \quad (\text{S16})$$

Similarly, we can derive the values for the overpotential at $\Delta G_{OH} = 1.23 \text{ eV}$ (the crossing point of the two volcanoes) and $\Delta G_{OH} = 1.60 \text{ eV}$ (the OER apex) as:

$$-\eta_{OER,2}(\Delta G_{OH} = 1.60 \text{ eV}) = \left(\frac{1.6 \text{ eV}}{e} - 1.97 \text{ V} \right) = -0.37 \text{ V} \quad (\text{S17})$$

$$-\eta_{OER,2}(\Delta G_{OH} = 1.23 \text{ eV}) = \left(\frac{1.23 \text{ eV}}{e} - 1.97 \text{ V} \right) = -0.74 \text{ V} \quad (\text{S18})$$

S3. Functional shape of the Bifunctional Index

With the functional forms for η_{OER} and η_{ORR} obtained in the previous section (Equations S12-S15), we can now explain the shape of the function that defines the bifunctional index (BI), as shown in Figure 2 in the main text. We reproduce here Figure 2 without the explicit datapoints

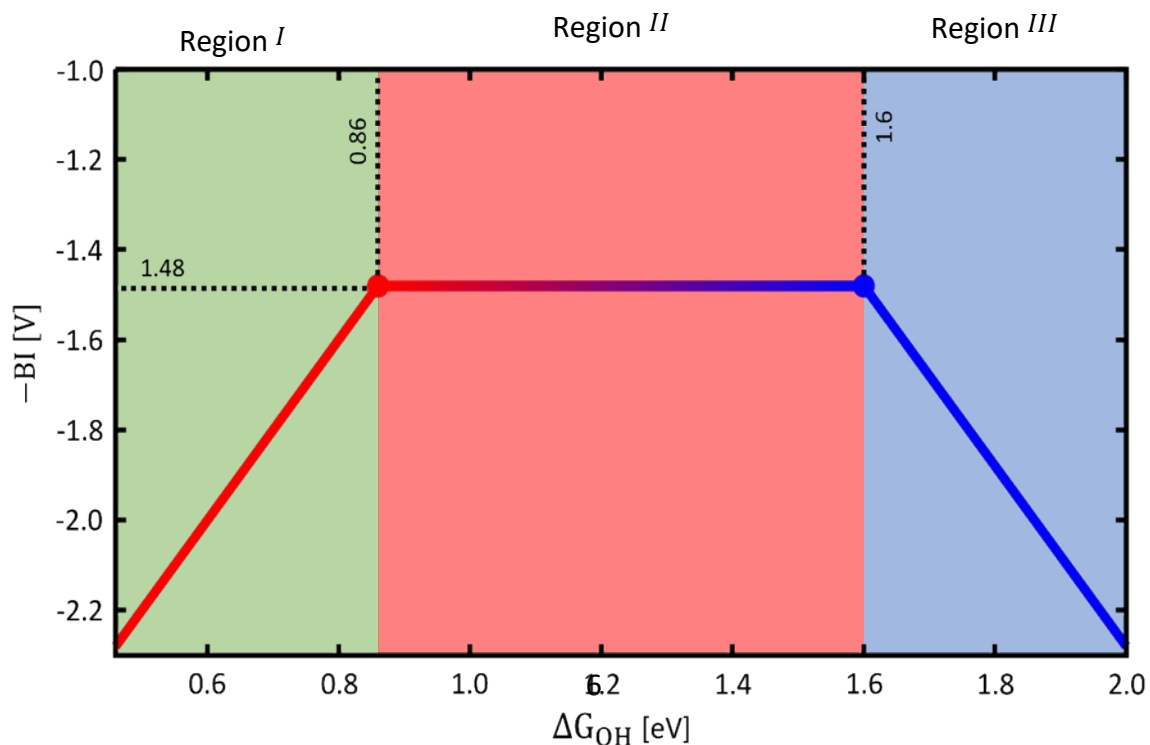


Figure S3. The Bifunctional Index (BI) as a function of ΔG_{OH} , reproduced from Figure 2 main text, with the equivalent regions from Figure S2, without the explicit datapoints.

as Figure S3. As noted in the main text, BI is computationally defined as the sum of the overpotentials for the OER and ORR:

$$BI = \eta_{OER} + \eta_{ORR} \quad (S19)$$

This means that there are again three regions, corresponding to the regimes in Figure S2 and Figure S3, in which:

- I. η_{OER} is decreasing and η_{ORR} is decreasing as ΔG_{OH} becomes increasingly positive, for $\Delta G_{OH} < 0.86 \text{ eV}$.
- II. η_{OER} is decreasing and η_{ORR} is increasing as ΔG_{OH} is made more positive, for $0.86 \text{ eV} < \Delta G_{OH} < 1.6 \text{ eV}$.
- III. η_{OER} is increasing and η_{ORR} is increasing alongside ΔG_{OH} , for $\Delta G_{OH} < 1.6 \text{ eV}$.

For these three regions, we can write BI as follows:

$$-BI_I = -\eta_{OER,-1} + \eta_{OER,2} = \frac{\Delta G_{OH}}{e} - 1.23 \text{ eV} + \frac{\Delta G_{OH}}{e} - 1.97 \text{ eV} = \frac{2\Delta G_{OH}}{e} - 3.20 \text{ V} \quad (S20)$$

$$-BI_{II} = -\eta_{OER,-4} + \eta_{OER,2} = -\frac{\Delta G_{OH}}{e} + 0.49 \text{ V} + \frac{\Delta G_{OH}}{e} - 1.97 \text{ V} = -1.48 \text{ V} \quad (S21)$$

$$-BI_{III} = -\eta_{OER,-4} + \eta_{OER,3} = -\frac{\Delta G_{OH}}{e} + 0.49 \text{ V} + -\frac{\Delta G_{OH}}{e} + 1.23 \text{ V} = -\frac{2\Delta G_{OH}}{e} + 1.72 \text{ V} \quad (S22)$$

From these equations it can also be seen that the minimum value for BI , if the catalyst follows the same scaling relations for both parts of the ORR/OER redox couple, is 1.48 V.

Lastly, we derive the scaling-relation-based limitation for BI , in case the catalyst has two active centres with different adsorption energies of $*O$, $*OH$ and $*OOH$. In this case, the two tops of the volcanoes for ORR and OER can be reached concurrently, which means that:

$$\eta_{OER} = \eta_{ORR} = 0.37 V \quad (S23)$$

which then leads to:

$$BI = \eta_{OER} + \eta_{ORR} = 0.37 V + 0.37 V = 0.74 V \quad (S24)$$

S4. Corrections for the datapoints in Figure 2 in the main text

Figure 2 in the main text contains the data points obtained from the publications of Pique et al⁴ on functionalized graphitic materials (FGMs), who in turn obtained them from Calle-Vallejo et al,⁵ as well as recent data by Niu et al.⁶ The shown datapoints contain two changes when comparing to the originally reported data:

- 1) The solvation correction was removed from the data on the FGMs.

The calculations in the works by Pique et al⁴ and Calle-Vallejo et al⁵ contained external, somewhat arbitrary, ad hoc solvation corrections for $*OH$ and $*OOH$ and neglected the solvation of $*O$, which was shown in later works to be important^{7,8} and similar in magnitude to those of $*OH$ and $*OOH$. Thus, here, we removed the solvation correction of $G_{solv} = -0.3 eV$ for ΔG_{OH} and ΔG_{OOH} from the shown data.

- 2) The data of Niu et al.⁶ were corrected to account for the fact that they were calculated using a different exchange-correlation functional.

Since the calculations of Niu et al were executed using PBE, while the ones on the FGMs were performed using RPBE, the adsorption energies and scaling lines for $*O$ vs $*OH$ do not match. Therefore, we shifted all the adsorption energies of $*OH$ by 0.37 eV, which is the average

horizontal difference between the scaling line of region I ($-BI_I = \frac{2\Delta G_{OH}}{e} - 3.20 V$, i.e., Equation S20) and the calculated datapoints in Figure S6. We note that the shift is used to modify only the descriptor (ΔG_{OH}), not the values of BI . Figure S6 shows the equivalent of Figure 2 in the main text, without the linear shift in ΔG_{OH} .

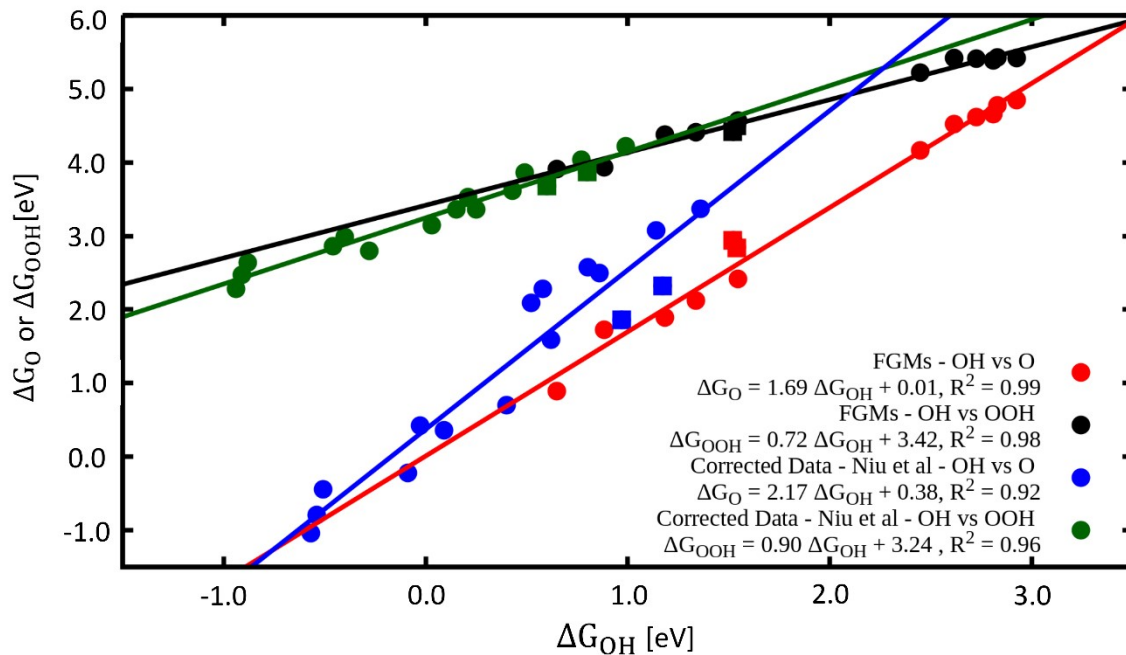


Figure S5. Scaling relations for the adsorption energies of *O , *OH and *OOH for the two datasets used in Figure 2 in the main text,⁴⁻⁶ including all corrections. In this version, the offset has been corrected and represents the final dataset used to generate Figure 2 in the main text and Figure S7. The anomalous datapoints discussed in Section S5 are marked with squares of the respective colours.

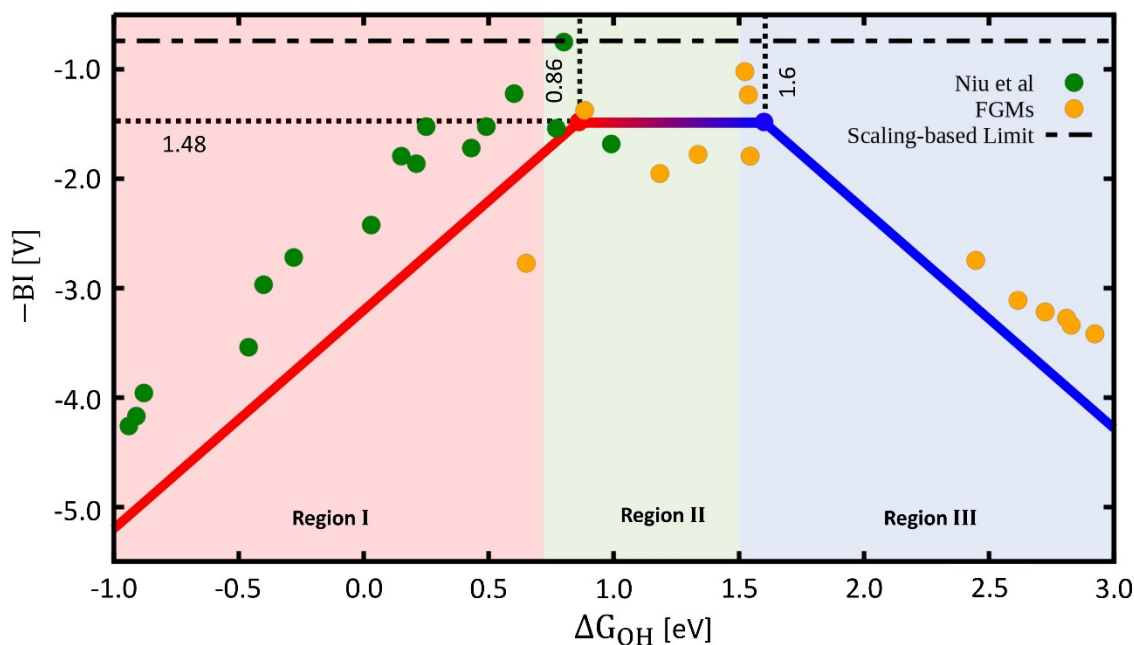


Figure S6. Additive inverse of the Bifunctional Index ($-BI$) as a function of ΔG_{OH} , as shown in Figure 2 in the main text. However, without the linear shift for the data of Niu et al.⁶

S5. Discussion of the anomalous datapoints in Figure 2 in the main text

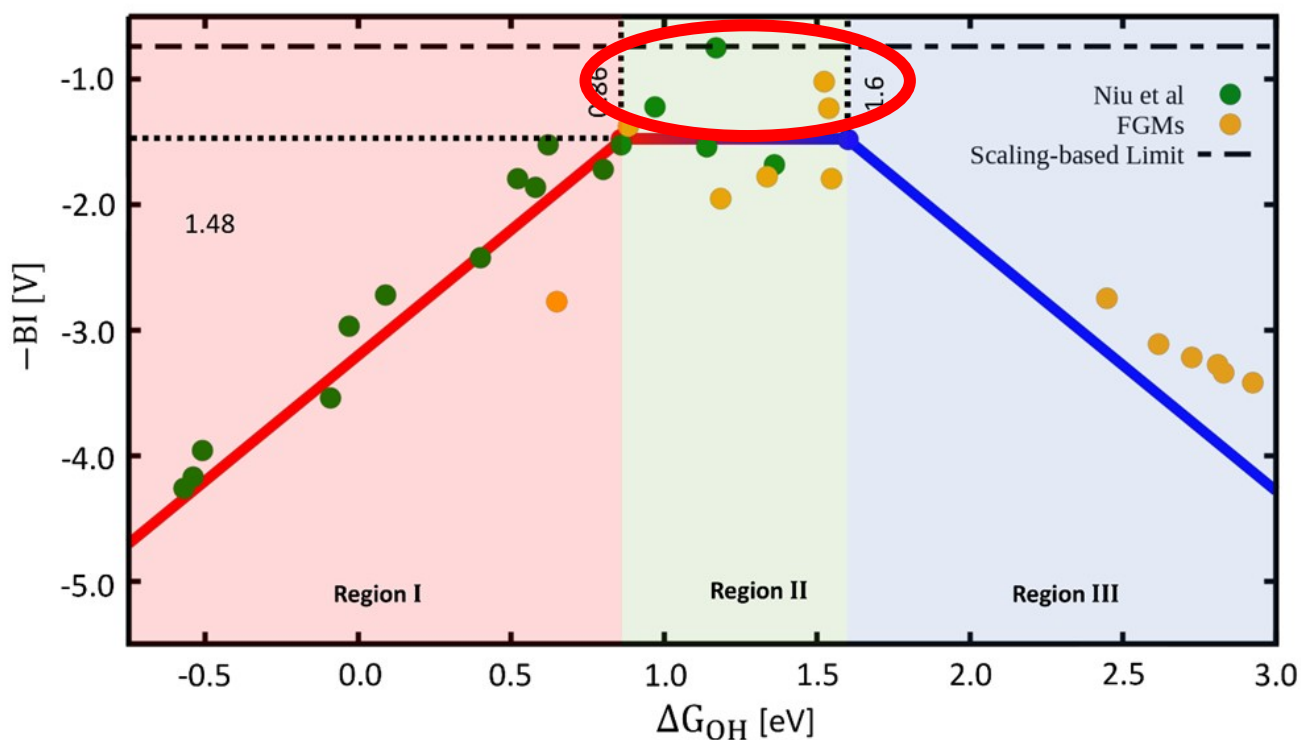


Figure S7. Reproduction of Figure 2, from the main text, with anomalous datapoints marked with a red circle.

In the following, we will discuss the behaviour and origin of the 4 anomalous datapoints found in Figure 2 in the main text, shown here as Figure S7, with the anomalous datapoints marked with a red circle. It is worth noting that two of the 4 datapoints are linked to FGM and a nitrogen-doped graphene catalysts in which the active site is a rhodium atom. The other two stem from a Co-based FGM and an Ir-based nitrogen-doped graphene catalyst.

The markedly low BI for these catalysts stems from their beneficial deviations, tabulated in Table S1, from the expected $*O$ vs $*OH$ scaling lines, as shown in Figure S4 and Figure S5. This would indicate that, due to their consistent advantageous deviations from the scaling lines in multiple environments, elements in group 9 of the periodic table (Co, Rh, Ir) seem to be interesting elements to further investigate for applications as bifunctional SACs.

Table S1. Anomalous catalysts, as described in the text, along with the ΔG_{OH} , ΔG_O , ΔG_{OOH} and their respective expected values, $\Delta G_{O,scal}$, $\Delta G_{OOH,scal}$, based on the scaling relations shown in Section S4 and ΔG_{OH} , as well as the differences between the actual and expected values.

Active sites	ΔG_{OH} (eV)	ΔG_O (eV)	$\Delta G_{O,scal}$ (eV)	$\Delta G_O - \Delta G_{O,scal}$ (eV)	ΔG_{OOH} (eV)	$\Delta G_{OOH,scal}$ (eV)	$\Delta G_{OOH} - \Delta G_{OOH,scal}$ (eV)
FGM-Co	1.52	2.94	2.58	0.36	4.42	4.51	-0.09
FGM-Rh	1.54	2.84	2.61	0.23	4.50	4.53	-0.03
NDG-Rh	0.80	2.32	2.91	-0.59	3.87	3.96	-0.09
NDG-Ir	0.60	1.86	2.48	-0.62	3.68	3.78	-0.10

S6. Explicit values for ΔG_{OH} , ΔG_O , ΔG_{OOH} , η_{OER} , η_{ORR} and BI, as shown in Figure 2 in the main text

Table S2. DFT-calculated datapoints on the FGMs^{4,5} shown in Figures 2 and S7. The anomalous datapoints discussed in the text are marked in orange.

FGMs – Metal Center	ΔG_{OH} (eV)	ΔG_O (eV)	ΔG_{OOH} (eV)	η_{OER} (V)	η_{ORR} (V)	BI (V)
Cr	0.65	0.89	3.91	1.79	0.99	2.77
Mn	1.18	1.89	4.38	1.26	0.69	1.95
Fe	1.34	2.12	4.41	1.06	0.72	1.78
Co	1.52	2.94	4.42	0.29	0.73	1.02
Ni	2.45	4.17	5.22	1.22	1.53	2.75
Cu	2.62	4.52	5.42	1.39	1.73	3.11
Ru	0.88	1.72	3.94	0.98	0.39	1.37
Rh	1.54	2.84	4.50	0.42	0.81	1.23

Pd	2.81	4.66	5.38	1.58	1.69	3.27
Ag	2.83	4.77	5.43	1.60	1.74	3.34
Ir	1.55	2.42	4.57	0.92	0.88	1.79
Pt	2.72	4.62	5.41	1.49	1.72	3.22
Au	2.92	4.85	5.42	1.69	1.73	3.42

Table S3. DFT datapoints from Niu et al⁶ shown in Figures 2 and S6. For ΔG_{OH} we provide both the uncorrected and the corrected values (with a constant shift of 0.37 eV, in parentheses), as described in Section S4. The anomalous datapoints discussed in the text are marked in orange.

NDGs – Metal Center	ΔG_{OH} (eV)	ΔG_O (eV)	ΔG_{OOH} (eV)	η_{OER} (V)	η_{ORR} (V)	BI (V)
Ti	-0.91 (-0.54)	-0.79	2.47	2.03	2.14	4.17
V	-0.94 (-0.57)	-1.04	2.28	2.09	2.17	4.26
Cr	-0.46 (-0.09)	-0.22	2.86	1.85	1.69	3.54
Mn	-0.40 (-0.03)	0.42	2.99	1.34	1.63	2.97
Fe	0.03 (0.40)	0.70	3.15	1.22	1.2	2.42
Co	0.25 (0.62)	1.59	3.36	0.54	0.98	1.52
Ni	0.15 (0.52)	2.09	3.36	0.71	1.08	1.79
Cu	0.77 (1.14)	3.08	4.04	1.08	0.46	1.54
Zr	-0.88 (-0.51)	-0.44	2.64	1.85	2.11	3.96
Ru	0.43 (0.09)	0.36	2.80	1.21	1.51	2.72
Rh	0.80 (1.17)	2.32	3.87	0.32	0.43	0.75
Pd	0.43 (0.80)	2.58	3.62	0.92	0.8	1.72
Ag	0.99 (1.36)	3.37	4.22	1.15	0.53	1.68
Ir	0.60 (0.97)	1.86	3.68	0.59	0.63	1.22
Pt	0.21 (0.58)	2.28	3.53	0.84	1.02	1.86
Au	0.49 (0.86)	2.50	3.86	0.78	0.74	1.52

S7. References

- 1 M. T. M. Koper, *J. Electroanal. Chem.*, 2011, **660**, 254–260.
- 2 I. C. Man, H. Su, F. Calle-Vallejo, H. A. Hansen, J. I. Martínez, N. G. Inoglu, J. Kitchin, T. F. Jaramillo, J. K. Nørskov and J. Rossmeisl, *ChemCatChem*, 2011, **3**, 1159–1165.
- 3 F. Abild-Pedersen, J. Greeley, F. Studt, J. Rossmeisl, T. R. Munter, P. G. Moses, E. Skúlason, T. Bligaard and J. K. Nørskov, *Phys. Rev. Lett.*, 2007, **99**, 16105.
- 4 O. Piqué, F. Illas and F. Calle-Vallejo, *Phys. Chem. Chem. Phys.*, 2020, **22**, 6797–6803.
- 5 F. Calle-Vallejo, J. I. Martínez and J. Rossmeisl, *Phys. Chem. Chem. Phys.*, 2011, **13**, 15639.
- 6 H. Niu, X. Wan, X. Wang, C. Shao, J. Robertson, Z. Zhang and Y. Guo, *ACS Sustain. Chem. Eng.*, 2021, **9**, 3590–3599.
- 7 F. Calle-Vallejo, A. Krabbe and J. M. García-Lastra, *Chem. Sci.*, 2017, **8**, 124–130.
- 8 M. Reda, H. A. Hansen and T. Vegge, *Catal. Today*, 2018, **312**, 118–125.